



Supplement of

Tropospheric warming over the northern Indian Ocean caused by South Asian anthropogenic aerosols: possible impact on the upper troposphere and lower stratosphere

Suvarna Fadnavis et al.

Correspondence to: Suvarna Fadnavis (suvarna@tropmet.res.in)

The copyright of individual parts of the supplement might differ from the article licence.

Supplementary material

2 Section S1: AOD satellite observations

In this study we use the last fifteen years (2001 – 2016) of aerosol optical depth at 0.55 μm (AOD) obtained from the Moderate Resolution Imaging Spectroradiometer (MODIS) instrument onboard the NASA EOS Terra satellite are used. The MODIS instrument measure a radiance in 36 spectral channels at a spatial resolution ranging from 250 m to 1 km with a 2300 km wide swath, allowing for almost daily global coverage. Terra MODIS (MOD08_M3 V6.1) AOD aerosol products are retrieved using the Deep Blue (DB) algorithm (Mhawish et al., 2019). The algorithm calculates the column aerosol loading at 0.55 μm over land and ocean. The AOD data from MODIS Terra can be downloaded from https://doi.org/10.5067/MODIS/MOD08_M3.061, 2017 AOD data from the Multi-angle Imaging Spectro-Radiometer (MISR) for the same period as MODIS (2001 – 2016) is also used for model evaluation (2020). The MISR sensor onboard the Terra satellite has been operational since 1999. It makes measurements at four spectral bands centered at 443 nm, 555 nm, 670 nm, and 865 nm (Diner et al., 2008). In this study we used, level 3 (MIL3MAE_v4) monthly mean aerosol optical depth at 555 nm wavelength at a spatial resolution of $0.5^\circ \times 0.5^\circ$. The MISR AOD data is available for download at <https://doi.org/10.5067/TERRA/MISR/MIL3MJTA.002>

20 Section S2:Model evaluation

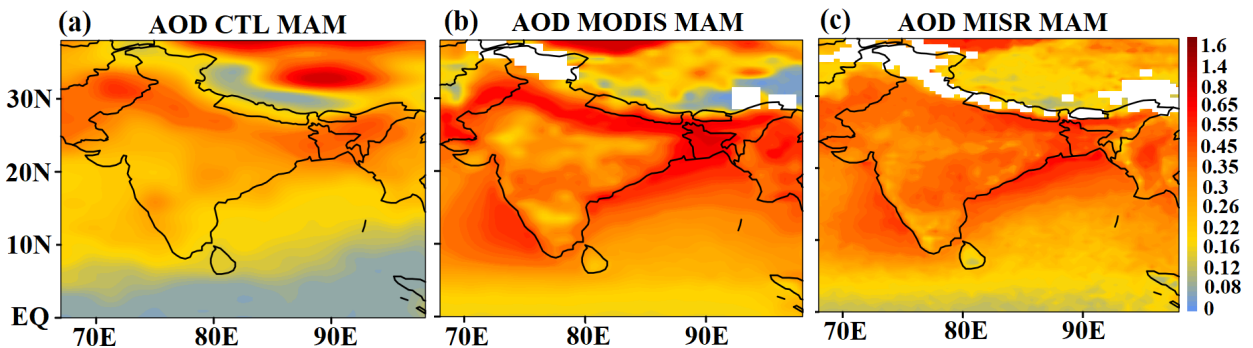
We evaluate the model performance by comparing simulated AOD (from CTL simulations) with MISR and MODIS data for the spring season. The model simulations show high amounts of AOD over the Indo-Gangetic plain (25° - 35° N, 75° - 95° E), consistent with MODIS and MISR observations, despite quantitative differences (Fig. S1). Compared to

25 observations, the model underestimates AOD over the Indo-Gangetic plain by ~18 % than
26 MODIS and overestimates by 14% than MISR. While it underestimates over central India
27 ($15^{\circ} - 24^{\circ}$ N, $75^{\circ} - 82^{\circ}$ E) by 20 – 23 % compared to MODIS and MISR. There are differences
28 among satellite observations and between the model and observations. The differences are
29 due to (1) uncertainties in the model transport processes, the emission inventory, and the
30 parameterizations. (Fadnavis et al. 2014, 2015, 2018, 2019) and (2) there are uncertainties in
31 the satellite measurements (Bibi et al., 2015). The comparison of AOD from Aerosol Robotic
32 Network (AERONET), MODIS and MISR show error of 0.03 to 0.05 (Kahn et al., 2007).
33 With model biases present in both the CTL and the perturbed simulations, investigating
34 anomalies removes some of the model bias. In the past Fadnavis et al. (2018, 2019, 2020,
35 2021a,b) reported model evaluations for AOD, absorbing aerosol index, precipitation, mixing
36 ratio of black carbon aerosol and cloud ice with various measurements.

37

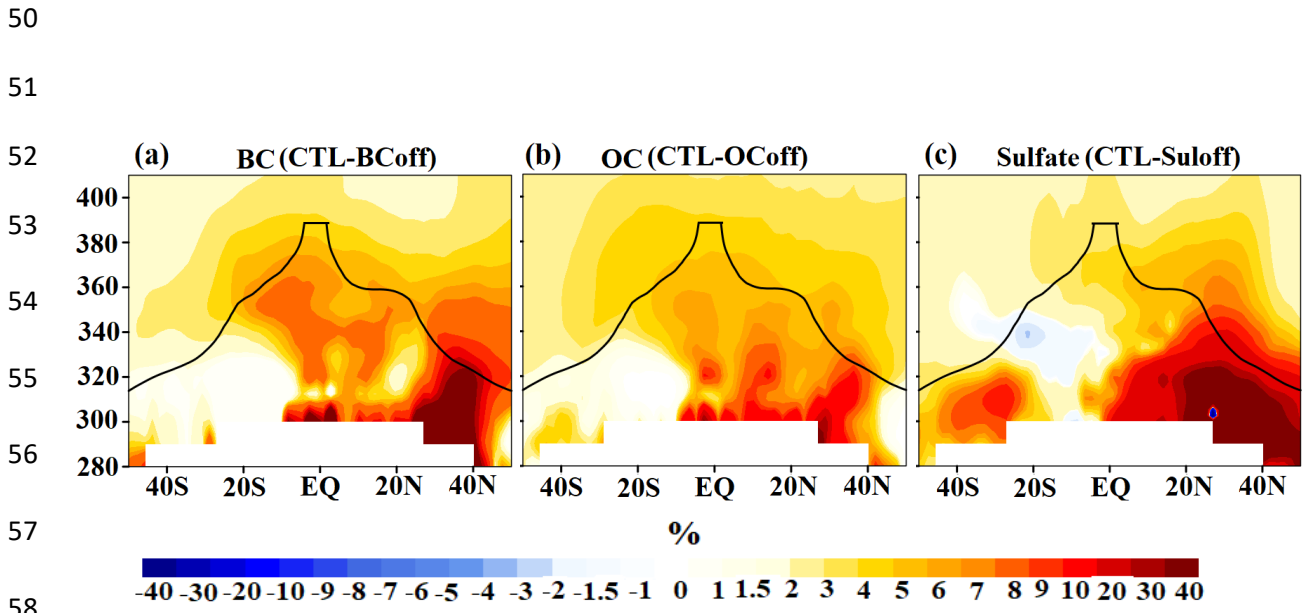
38

39



45 Figure S1: Spatial distribution of AOD average for the spring season for the years 2001 – 2016,
46 from (a) ECHAM6-HAMMOZ CTL simulations, (b) MODIS measurements average for the
47 spring season during 2001 – 2016, (c) MISR measurement average for the spring season during
48 2001 – 2016.

49



59 Figure S2: 4: Meridional cross-section over Indian Ocean-western Pacific (averaged 30° E –
60 140° E and for the spring season for the years 2001 – 2016) of anomalies (%) for (a) BC aerosols
61 from CTL-BCoff simulations, (b) OC aerosols from CTL-OCoff simulations, (c) sulfate
62 aerosols from CTL-Suloff simulations. A black line in Figs. a-c indicates the dynamical
63 tropopause.

64
65
66
67
68

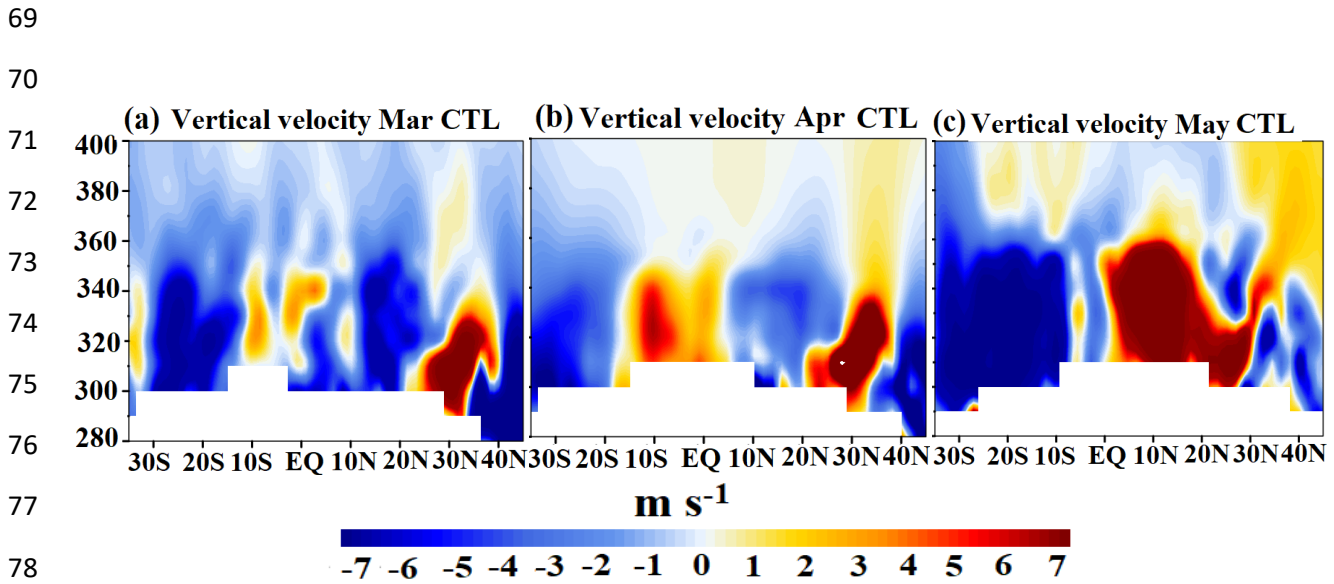


Figure S3: Meridional section of vertical velocities (CTL simulations) for (a) March, (b) April, (c) May, averaged during 2001 – 2016 and over the North Indian Ocean – Western Pacific (65° E – 140° E) (the vertical velocity field has been scaled by 300 and the units are m s^{-1}).

87

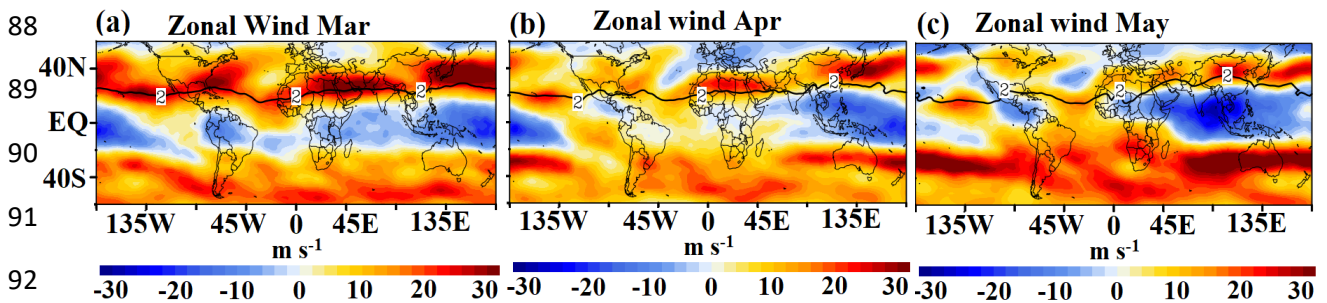


Figure S4: Zonal wind (m s^{-1}) at 360 K potential temperature level from CTL simulations for (a) March, (b) April, (c) May. The potential vorticity (2 PVU) is indicated by the black contour.

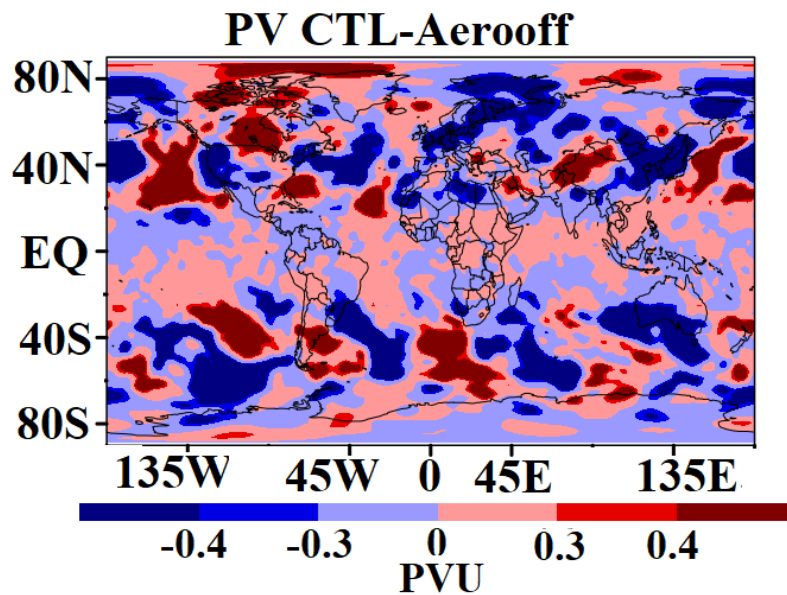


Figure S5: Spatial distribution of anomalies (CTL-Aerooff) of Potential vorticity (PVU) ($1 \text{ PVU} = 10^{-6} \text{ m}^2 \text{ kg s}^{-1}$) averaged for spring and 350-360K potential temperature levels.

114

115 Table-S1: Mean radiative forcing (W m^{-2}) (averaged for spring) at the Top of the
 116 Atmosphere (TOA), surface (Surface) and In-atmosphere (TOA- Surface) averaged over the
 117 Indo-Gangetic Plan (IGP, Lon:75 – 83 $^{\circ}$ E, lat: 26 – 30 $^{\circ}$ N), Arabian Sea (A.S.: lon: 55 – 70 $^{\circ}$
 118 E, lat: 8 – 20 N), and Bay of Bengal (BoB) (Lon:88 – 92 $^{\circ}$ E, lat:12 – 20 $^{\circ}$ N) from all aerosols
 119 (CTL -Aerooff), BC (CTL - BCoff), OC (CTL - OCoff) and sulfate (CTL - Suloff).

CTL-Aerooff			
	TOA (W m^{-2})	Surface (W m^{-2})	In-atmosphere (W m^{-2})
IGP	1.27±0.16	-11.16±0.50	12.44±0.42
A.S	-0.72±0.14	-3.009±0.28	2.27±0.19
BoB	-1.24±0.15	-5.14±0.44	3.89±0.30
CTL-BCoff			
IGP	4.33±0.17	-9.27±0.37	13.61±0.44
A.S	1.24±0.13	-2.56±0.25	3.81±0.23
BoB	1.54±0.26	-3.70±0.49	5.25±0.39
CTL-OCoff			
IGP	-0.44±0.15	-2.56±0.45	2.12±0.42
A.S	-0.216±0.13	-0.49±0.31	0.27±0.10
BoB	-0.41±0.20	-0.79±0.34	0.38±0.19
CTL-Suloff			
IGP	-1.62±0.18	-2.67±0.36	1.05±0.30
A.S	-1.55±0.16	-1.19±0.24	-0.36±0.10
BoB	-2.14±0.17	-2.04±0.44	-0.095±0.032

120

121

122

123

124 **References:**

- 125 Bibi, H., Alam, K., Chishtie, F., Bibi S., Shahid, I, Blaschke, T., Intercomparison of MODIS,
126 MISR, OMI, and CALIPSO aerosol optical depth retrievals for four locations on the
127 Indo-Gangetic plains and validation against AERONET data, Atmospheric Environment,
128 111, 113-126, <https://doi.org/10.1016/j.atmosenv.2015.04.013>, 2015.
- 129 Diner, D. J., Abdou, W. A., Ackerman, T. P., Crean, K., Gordon, H. R., Kahn, R. A.,
130 Martonchik, J. V., Mcmurdoch, S., Paradise, S. R., Pinty, B., Verstraete, M. M., Wang,
131 M., West, R. A. Level 2 aerosol retrieval algorithm theoretical basis, Jet Propuls. Lab.
132 Intern. Doc. JPL D-11400, Rev C, 2008.
- 133 Fadnavis, S., Kalita, G., Rowlinson, M., Rap, A., Li, J.-L. F., Gasparini, B., Laakso, A. and
134 Müller, R.: The impact of increases in South Asian anthropogenic emissions of SO₂ on
135 sulfate loading in the upper troposphere and lower stratosphere during the monsoon
136 season and the associated radiative changes, Atmos. Chem. Phys., 19, 9989–10008,
137 <https://doi.org/10.5194/acp-19-9989-2019>, 2019.
- 138 Fadnavis, S., Roy, C., Chattopadhyay, R., Sioris, C. E., Rap, A., Müller, R., Kumar, K. R. and
139 Krishnan, R.: Transport of Asian trace gases via eddy shedding from the Asian summer
140 monsoon anticyclone and associated impacts on ozone heating rates, Atmos. Chem.
141 Phys., 18, 11493–11506, doi:10.5194/acp-18-11493-2018, 2018.
- 142 Fadnavis S., Semeniuk K., Schultz M.G., Kiefer M., Mahajan A., Pozzoli L., Sonbawane S.,
143 Transport pathways of peroxyacetyl nitrate in the upper troposphere and lower
144 stratosphere from different monsoon systems during the summer monsoon season,
145 Atmospheric Chemistry and Physics, 15, 11477-11499, DOI:10.5194/acp-15-11477-
146 2015, 2015.
- 147 Fadnavis S., Schultz M.G., Semeniuk K., Mahajan A.S., Pozzoli L., Sonbawane S., Ghude

148 S.D., Kiefer M., Eckert E., Trends in Peroxyacetyl Nitrate (PAN) in the upper
149 troposphere and lower stratosphere over Southern Asia during the summer monsoon
150 season: regional impacts., Atmospheric Chemistry and Physics, 14, 12725-12743,
151 DOI:10.5194/acp-14-12725-2014, 2014.

152 Fadnavis, S., Sioris, C. E., Wagh, N., Chattopadhyay, R., Tao, M., Chavan, P. and Chakroborty,
153 T.: A rising trend of double tropopauses over South Asia in a warming environment:
154 Implications for moistening of the lower stratosphere, Int. J. Climatol., 41, E200–E215,
155 doi:10.1002/joc.6677, 2020.

156 Fadnavis, S., Sabin, T. P., Rap, A., Müller, R., Kubin, A. and Heinold, B.: The impact of
157 COVID-19 lockdown measures on the Indian summer monsoon, Environ. Res. Lett.,
158 16, 074054, doi:10.1088/1748-9326/ac109c, 2021a.

159 Fadnavis S., Müller R , Chakraborty T. , Sabin T. P., Laakso A. , Rap A. , Griessbach S.,
160 Vernier J-P., and Tilmes S., The role of tropical volcanic eruptions in exacerbating
161 Indian droughts, Sci. Rep., 11, 2714, doi.org/10.1038/s41598-021-81566-0, 2021b.

162 Kahn, R. A., Garay, M. J., Nelson, D. L., Yau, K. K., Bull, M. A., Gaitley B. J., Martonchik,
163 J. V., and Levy, R. C.: Satellite-derived aerosol optical depth over dark water from MISR
164 and MODIS: Comparisons with AERONET and implications for climatological studies,
165 J. Geophys. Res., 112, D18205, doi:10.1029/2006JD008175, 2007.

166 Mhawish, A. T., Banerjee, M., Sorek-Hamer, A., Lyapustin, D., Broday, and Chatfield, R.:
167 Comparison and Evaluation of MODIS Multi-Angle Implementation of Atmospheric
168 Correction (MAIAC) Aerosol Product over South Asia, Remote Sens. of Environ., 224,
169 12–28, 2019.

170